5-5-1986

The Study of Biominerals by High Resolution Transmission Electron Microscopy

Stephen Mann
University of Bath

Utah State University
MERRILL-CAZIER LIBRARY

THE STUDY OF BIOMINERALS BY HIGH RESOLUTION TRANSMISSION ELECTRON MICROSCOPY

Stephen Mann

School of Chemistry
University of Bath
Claverton Down
Bath BA2 7AY
U.K.
Phone no.: 0225-826122

Abstract

This paper presents an overview of the study of the ultrastructure of biogenic inorganic solids (biominerals) using high resolution transmission electron microscopy (HRTEM). A range of biominerals have been studied including iron oxides, calcium phosphates, calcium carbonates and silica. The studies have revealed information concerning the structural complexity of these materials and have identified crystallographic order and disorder at the nanometre level. In addition, the results have aided the elucidation of the mechanisms of nucleation and growth of biogenic minerals.

Introduction

Although the study of the structure and growth of inorganic solids is regarded as being of importance and value in the fields of chemistry, materials science and physics it is not generally appreciated within these disciplines that inorganic solids play an important and fundamental role in the structure and function of living organisms. In addition, physical scientists involved in the structural characterization of inorganic solids and their modification for technological application (ceramics, magnetic and electronic devices, etc.) have not generally recognised the enormous potential for understanding and developing their studies through the investigation of biogenic solids. In particular, the central objective of technologically-based solid state science, viz the precise reproduction and tailoring of inorganic structures for functional end-use, has been achieved, albeit within a limited range of materials, through the eons of biological evolution.

Biogenic inorganic solids (biominerals) are formed through biological reactions which are characterised by high selectivity and precision. Furthermore, the inherent regulation and control of these processes results in well-defined, reproducible crystallochemical properties. For example, crystallite size, morphology, growth direction, structure and crystallographic orientation can all be precisely determined in unique and novel arrangements. These aspects of stereo, chemical and structural specificity arise from the control of nucleation and growth processes and are important criteria in the development and design of novel synthetic routes to inorganic materials.

This paper presents an overview of the study of the ultrastructure of biominerals using high resolution transmission electron microscopy (HRTEM). These investigations have only recently been undertaken. The aim of this paper is to highlight the major results arising from HRTEM investigations, attempting to place them into their appropriate biological context in order to give the reader an insight into the fascination and complexity of biomineralization processes.

Although over forty biominerals are now known in extant organisms (Lowenstam 1981) only a few

have been studied by HRTEM. These include; iron oxides (magnetite, goethite and ferrihydrite), calcium phosphates (hydroxyapatite, and amorphous phases) calcium carbonates (calcite and aragonite) and amorphous silica. The studies have greatly aided our understanding concerning the structure and formation of biomineralized phases. They have provided information on the structural complexity of these solids, identifying crystal domain sizes and imperfections such as defects, dislocations, lowering of space group symmetry and amorphous microdomains. In addition, the identification of nucleation sites, preferred growth directions, amorphous precursors and unique morphological states, in conjunction with data obtained from other physical techniques (polarised light microscopy, infrared spectroscopy, X-ray diffraction, TEM and SEM), has significantly advanced the elucidation of the mechanisms of nucleation and growth of biogenic minerals.

We begin by an introduction into the technique of HRTEM, its potential and difficulties. The paper then progresses through various biomineralization systems involving both crystalline and amorphous phases. A detailed account of the fundamental chemical concepts involved in biomineralization reactions is discussed elsewhere (Mann 1983).

Instrumentation: High Resolution Transmission Electron Microscopy(HRTEM)

Since the early seventies HRTEM has become an established method for investigating the local structure of crystalline, pseudo-crystalline and amorphous materials at the nanometre level. It has been applied to the study of a wide variety of inorganic minerals (Hutchison et al. 1977) and, more recently, to the investigation of biogenic inorganic solids as reviewed in this paper.

The general applications of HRTEM in solid state chemistry are summarized in figure 1. The general aim is to investigate the structure and properties of materials through direct imaging of the crystal lattice in the electron microscope. In this way information concerning the nucleation and growth of materials can be studied and deviations from ideality in structure and stoichiometry elucidated.

The potential of HRTEM lies in the principle that for crystals of sufficient thickness (often less than 100A) the phase contrast observed in an electron micrograph recorded under specific conditions of defocus (Schwerzer defocus) is closely related to the projection of the atomic potential distribution in the crystal. In such ideal circumstances there is a one-to-one correspondence between the object under study and recorded image. However, in practice, the interpretation of high resolution electron micrographs is more difficult due to the sensitivity of such images to microscope aberrations, sample thickness (multiple scattering effects), and defocus conditions. These factors can be accommodated in theoretical
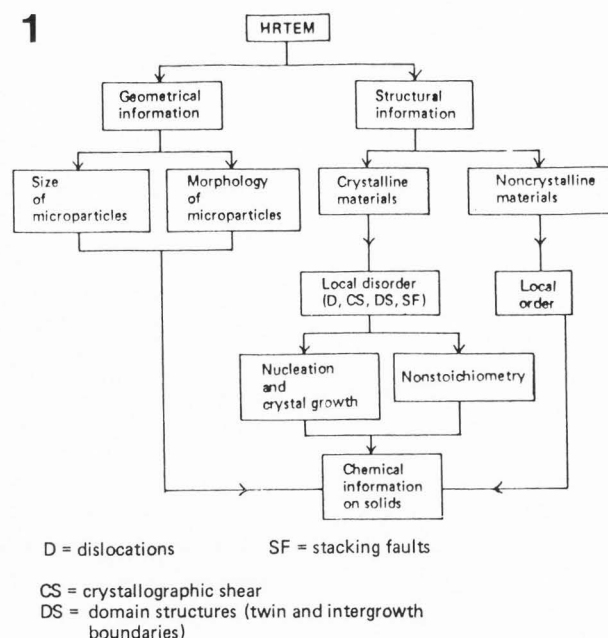

Figure 1. Flow diagram showing the general application of HRTEM in the study of solids.

calculations of image contrast such that the experimental and simulated images can be directly compared allowing evaluation of the information transferred from the object to recording plate in the electron microscope.

The combination of HRTEM and selected area electron diffraction (or other electron microdiffraction techniques) provides a means of studying individual micro-crystals such as the magnetite particles synthesised in magnetotactic bacteria (see below; Magnetotactic bacteria). In this way information concerning the nucleation and growth of individual crystals can in principle be deduced. No such information can be obtained from conventional structure-determination techniques such as X-ray diffraction since the data obtained is statistical in nature. However, care must be taken in the inference of general mechanisms of crystal formation from lattice images since not only may there be problems in interpretation but only a small fraction of the total sample population will be chosen for investigation and questions concerning the selectivity of the experimental data must be addressed.

Lattice fringes will only be observed when they lie in the Bragg orientation for diffraction and thus the absence of lattice images in a recorded image does not necessarily imply an amorphous structure but often an unaligned sample. Regions of local disorder within periodic arrays of atoms can be recognised by modulation of the lattice fringes although variations in crystal thickness and local crystal bending can have similar effects.

There may be several problems facing the study of biominerals using HRTEM. Firstly the materials may be too thick for high resolution

two-dimensional lattice images to be obtained. For example the HRTEM images obtained from bacterial magnetite crystals (see below; Magnetotactic bacteria) are generally too thick except at very thin edges for structure images to be resolved. In general only one dimensional lattice fringes are observed. In ultra thin (<100A) biomineral samples, such as the ferritin cores discussed below (Iron storage proteins) and calcium phosphate enamel crystals (see below; Human tooth enamel), two-dimensional images are possible. Under these circumstances the crystals are imaged at several different defocus conditions such that a 'through-focus' series of micrographs are recorded, with the optimum defocus position often around -650A. In this way the change of image structure with focus position can be evaluated. A powerful development in interpretation of these serial images is in the use of computer generated images under defined conditions of defocus, sample thickness and number of reflected beams comprising the final image. These multislice calculations (Cowley and Moodie 1957) are usually performed using programs developed by Lynch and O'Keefe (1972) and Skarnulis (1979). The importance of these simulations is illustrated below (Human tooth enamel) in which the comparison of experimental and theoretical results on human enamel hydroxyapatite reveals a change of hexagonal to monoclinic symmetry in microdomains within the structure.

A second problem is that many biominerals are intimately associated (often at the molecular level) with organic phases which are rapidly destroyed under the electron beam. Thus the original crystallographic orientations may be lost under examination. Biogenic calcium carbonates (see below; Gravity sensors) in particular, appear to be sensitive to localised beam heating.

A final problem involved in the study of biominerals by HRTEM is in the structural artefacts caused by sample preparation. Isolation procedures which involve crushing, oxidation, pH digestion, sectioning and staining can all interfere with or modify crystallochemical properties. The minimum treatment to attain samples for imaging should always be preferred. The HRTEM study of bacterial magnetite crystals within unfixed, intact cells (see below; Magnetotactic bacteria) is an excellent example of results which can be obtained from an unperturbed biological system (except for the high vacuum of the electron microscope).

Biominerals studied by HRTEM

Iron oxides. It is known that iron oxide deposition in organisms is widespread having been reported in all five living Kingdoms ranging from Animalia to Monera (Lowenstam 1981; Mann 1983; Webb 1983). HRTEM has been used to study three biological systems which utilise different structural types of iron oxide for different functional roles. These studies have been very successful in elucidating the crystallographic structure, degree of order, morphology and crystal growth mechanisms. The materials studied include (i) magnetite (Fe_3O_4) synthesis in magnetotactic bacteria, (ii) ferrihydrite formation ($5Fe_2O_3$ $9H_2O$) in the protein ferritin, and (iii) goethite (α-FeOOH) formation in limpet teeth.

Magnetite is a mixed valence iron oxide ($Fe^{II}Fe_2^{III}O_4$) with a cubic (Fd3m) inverse spinel structure in which the oxygen atoms are cubic close packed, all the Fe(II) ions are in octahedral sites, and half of the Fe(III) ions are in octahedral sites and half in tetrahedral interstices. Goethite is an iron(III) oxyhydroxide with an orthorhombic (Pnma) space group. Anions (O,OH) are hexagonally close packed and Fe(III) ions sited in octahedral holes. Iron atoms are arranged in such a way as to form double chains of $Fe(O,OH)_6$ octahedra which are linked by edge sharing along [001]. The double chains are held together by hydrogen bonds along [100]. Ferrihydrite is a poorly-ordered crystalline material, often non-stoichiometric, with a hexagonally close packed lattice of $O/OH/OH_2$ atoms with Fe(III) ions in octahedral sites. The octahedra are arranged similarly to those in hematite but the unit cell has only four instead of six octahedral layers in the $\underline{c}$ direction (Towe and Bradley 1967).

Magnetotactic bacteria. Three different sources of bacterial magnetite have been studied by HRTEM (Mann et al 1984 a, b; Matsuda et al. 1983). These include a cultured spirillum Aquaspirillum magnetotacticum, (Blakemore et al.1979), coccoid cells enriched from a complex simulated natural environment (Moench and Konetzka 1978) and an unidentified bacterium collected from pond mud (Matsuda et al. 1983). The cells of Aquaspirillum magnetotacticum are approximately 3 μm in length and contain, on average, 20 intracellular enveloped cubic magnetite particles, termed magnetosomes, of diameter 40-50 nm which are organized in a single chain that traverses the cell longitudinally (Balkwill et al 1980). Cells of A. magnetotacticum synthesise Fe_3O_4 only under microaerobic conditions accumulating Fe some 20,000-40,000 fold over the extracellular concentration (Blakemore et al. 1979). Magnetococcus cells are spherical bodies (ca 3 μm) and contain magnetite crystals enclosed within an organic membrane. The crystals are rectangular when viewed at low magnification with mean dimensions 100nm x 60nm (Towe and Moench, 1981). Although the crystals are sometimes located in ordered chains the most favourable configuration appears to be random. Crystals examined from the unidentified source were rectangular in morphology when viewed at low magnification with dimensions 60nm x 90nm. There appeared to be some alignment of the crystals within the elongated cells.

HRTEM has been used to study the following questions concerning bacterial magnetite: (a) what is the crystallographic nature of the individual crystals?; (b) what is the crystal morphology of these particles?, and (c) how do the crystals grow?. The general experimental

strategy has involved the direct lattice imaging of magnetite crystals in situ such that many of the potential artefacts associated with isolation techniques could be eliminated. A wide range of particles at different stages of development within the cell have been examined and compared and the crystallographic orientation in situ and the extent of crystallization in any one single chain has been evaluated.

All three samples when studied by HRTEM showed lattice images consistent with the magnetite structure. Fringe spacings corresponding to {111}, {222}, {220}, {200}, {400}, {311} were observed. In each bacterial magnetite studied the mature particles were identified as single domain crystals as shown by well defined lattice images which traversed the particles without any evidence of discontinuity or distortion (figures 2,3,and 4). Thus the particles were well ordered and essentially free from dislocations and stacking faults.

Although electron diffraction patterns were obtained on several crystals (figure 5) the zone of projection of the crystals was usually identified by consideration of the relative orientation of sets of fringes within the image. For example the crystal image in figure 2 is observed down the [01$\bar{1}$] direction. In this way, and by recording images from different projections, identification of the crystal faces could be attained and ultimately the three dimensional morphology of the crystals could be inferred.

Figure 6 shows the three different crystal morphologies adopted by the spirillum, coccus and unidentified cells respectively. The spirillum crystals have a habit based on an octahedron of {111} faces truncated by {100} faces. This is a typical inorganic crystal form for Fe_3O_4. In contrast both the coccoid and unidentified species have novel habits based on a hexagonal prism of {011} faces. The former has a complex arrangement of {100} and {011} truncated faces with the end {111} faces perpendicular to the threefold centrosymmetric axis. The unidentified species has a different set of truncated faces all being {111} in form. In each of these morphologies the direction of crystal alignment often coincides with the primary axis for magnetization, viz the [111] zone, and therefore optimises the magnetic moment within the cells.

HRTEM was also used to study the ultrastructure of immature bacterial magnetite particles providing insight into the nucleation and growth of these biogenic materials. Many crystal chains in A. magnetotacticum comprised crystals with marked variations in size and morphology ranging from particles with the characteristic cubo-octahedral habit of mature crystals through distorted forms to very irregular particles of sizes in the range of 10-30 nm. No linear sequence of crystallographic development along the chain could be observed by HRTEM imaging although crystals at the ends of the chains often appeared to be smaller in dimension.

Lattice imaging of the irregular particles showed the presence of contiguous crystalline and non-crystalline regions within magnetosomes of this type (figure 7). The crystalline zone was always observed to be single domain with well ordered lattice planes of magnetite. No other crystalline phases, such as γ-FeOOH, were observed. As can be seen in figure 7 the lattice fringes often appeared to extend into the amorphous region in a preferential direction which may indicate a preferred nucleation and growth direction. These multi-phase particles probably represent the early stages of magnetite formation with the non-crystalline material corresponding to the hydrated ferric oxide phases also identified by Mössbauer spectroscopy (Frankel et al. 1983).

In a similar way, many crystals isolated from the magnetotactic coccus cells did not show the well defined crystallographic morphology shown in figure 2. Other crystals showed high resolution images which had rounded edges and regions of discontinuity in the lattice fringes traversing the crystal zone. However, these crystals appeared to be structurally perfect since through-focus imaging showed that the seemingly atomic irregularities were in fact due to rapidly changing diffraction conditions due to variations in crystal thickness and not due to structural disorder in the crystal. Thus these highly ordered crystals appear to have extensive surface disorder. Figure 8 shows such a crystal imaged in the [01$\bar{1}$] zone. Careful examination of the micrograph indicated that the (011) lattice planes were regularly ordered within the crystal but were very low in contrast disappearing at the edges except in the [011] direction. These results suggest that there is extensive non-crystalline material overlying the crystal surface. It is unlikely that these images result from electron beam damage to the crystal since images and diffraction patterns did not change appreciably with time during the period of recording the micrographs.

On the basis of these HRTEM results and in the light of Mössbauer spectroscopy data (Frankel et al.1983) a working model for bacterial magnetite formation has been proposed (Mann 1985). The unique stage in the proposed sequence of events is the phase transformation of a hydrous ferric oxide sited within the magnetosome envelope to magnetite.

Iron storage proteins. The storage and mobilization of surplus iron in eukaryotes and some prokaryotes is regulated by the iron storage protein, ferritin. Ferritin isolated from horse spleen consists of a hollow spherical shell of 24 symmetrically related protein subunits (ca 18kDa per subunit) surrounding a core of inorganic hydrated iron (III) oxide (Ford et al. 1984). Phosphate (atomic ratio, Fe/Pi = 9 (Michaelis et al. 1943) may be associated with the surface of the iron oxide core in horse ferritin (Fischbach et al. 1969), (Treffry and Harrison, 1978), but does not appear to be a critical factor for core formation in reconstituted ferritins (Treffry and Harrison 1978; Macara et al. 1972). The volume of the cavity set by the protein shell is of the order of 70-80A resulting in an upper limit of 4500 iron atoms (ca 30% wt/wt Fe) which can be stored within the molecule. Typically, iron levels are high (10-20%) but variable.
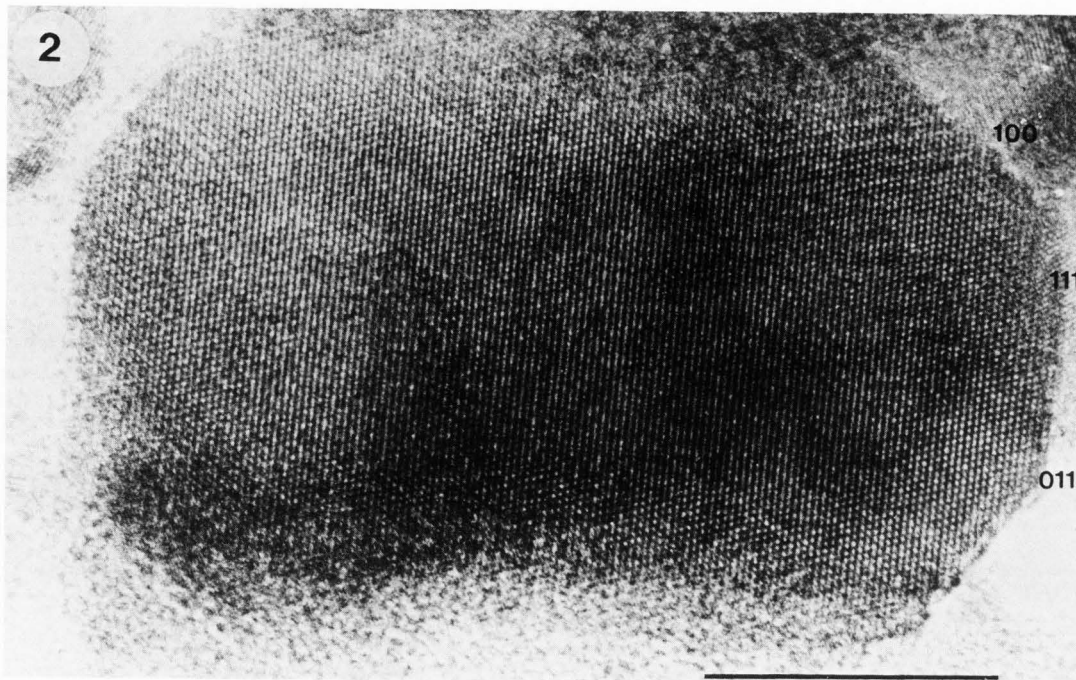
Figure 2. HRTEM image of a magnetite crystal isolated from coccoid cells imaged in the [01$\bar{1}$] zone. The crystal is well-ordered and has characteristic truncated faces. Bar = 20 nm.
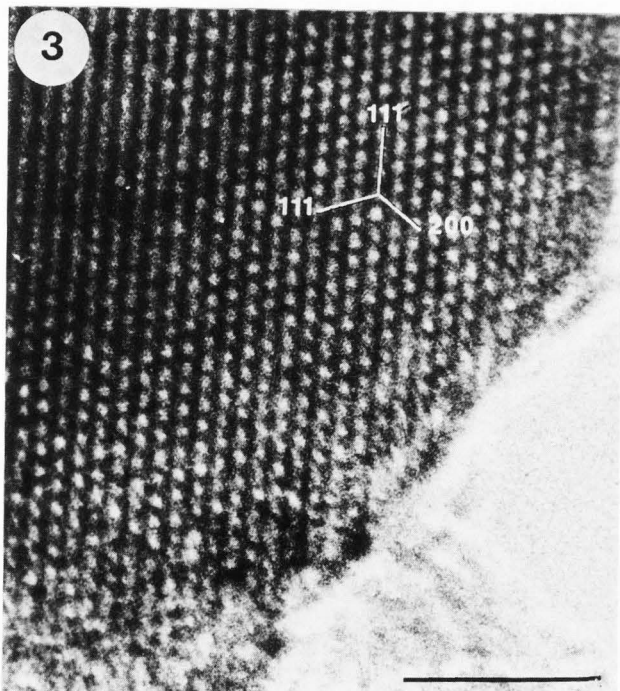

Figure 3. Enlarged micrograph of the [01$\bar{1}$] zone in figure 2 showing lattice fringes corresponding to (111), ($\bar{1}$11) and (200) planes. Bar = 5 nm.
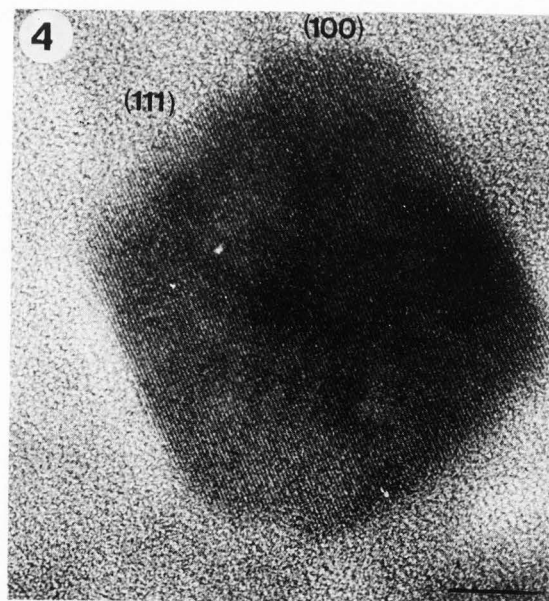

Figure 4. HRTEM image of a magnetite crystal recorded in situ within a cell of A. magnetotacticum. The crystal lies in the [01$\bar{1}$] zone, is well ordered, and has characteristic ({100} and {111}) truncated faces. Lattice fringes correspond to the (111) planes. Bar = 10 nm.
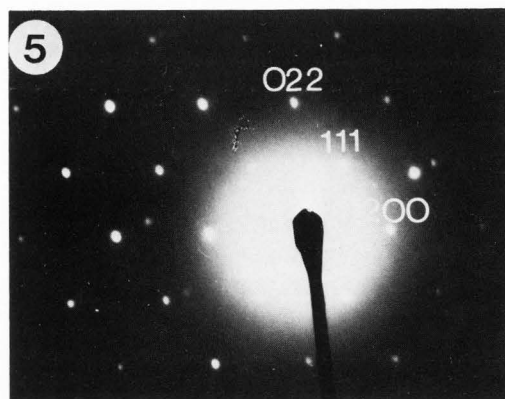
Figure 5. Selected area electron diffraction pattern from a mature magnetite crystal from A. magnetotacticum. The single crystal pattern corresponds to the $[01\bar{1}]$ zone. The (200) and $(\bar{2}00)$ reflections arise from double diffraction.
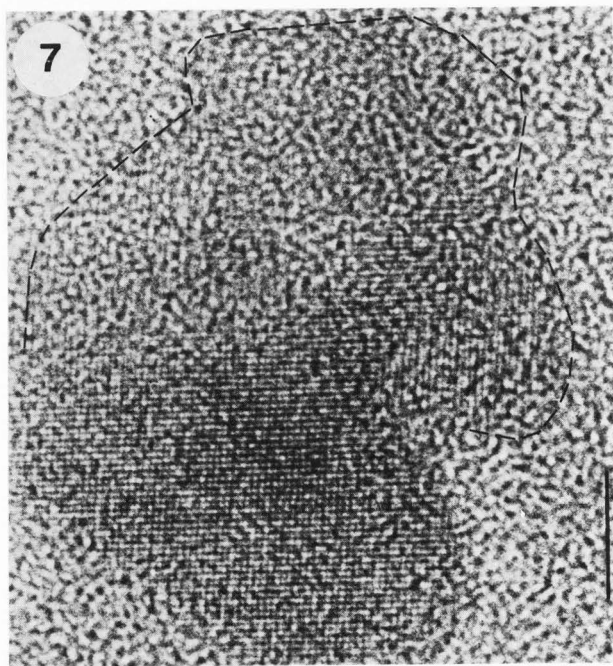

Figure 6. Idealised morphologies for mature bacterial magnetite crystals; a A. magnetotacticum; b, coccoid cells, and c, unidentified bacterium

Figure 7. Irregular, immature particle imaged in situ within a spirillum cell. The crystalline zone shows well-ordered (222) lattice fringes and is a single domain. An amorphous zone is coexistent with the crystalline domain. The superimposed black dashed line indicates the extent of the low contrast edge of the particle against the background carbon noise of the grid. Bar = 5 nm.
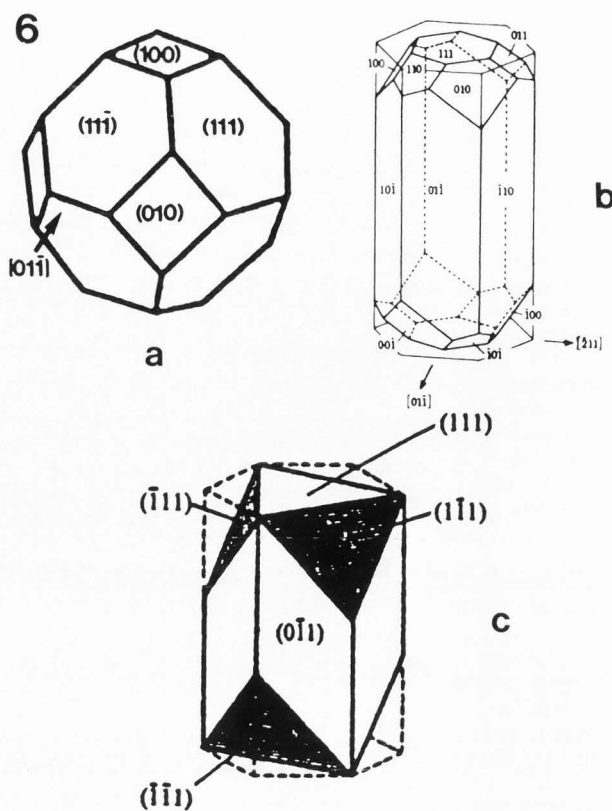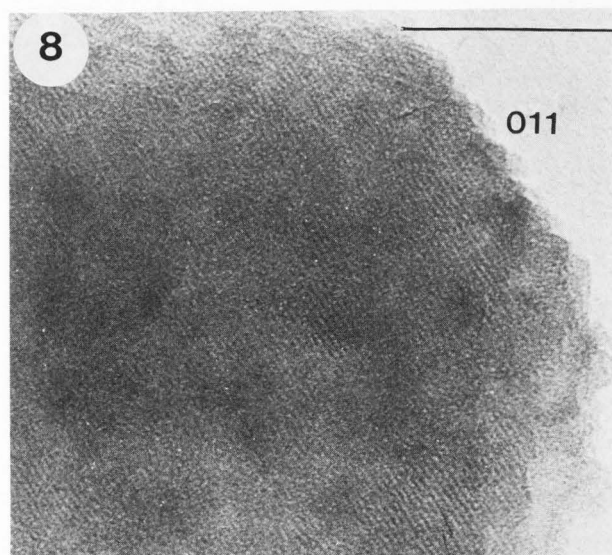

Figure 8. Magnetite crystal isolated from coccus cells imaged along $[01\bar{1}]$ and showing (011) lattice planes. Extensive non-crystalline material overlies the crystal surface. Bar = 20 nm.

Figures 9-12. HRTEM images of heat-treated and
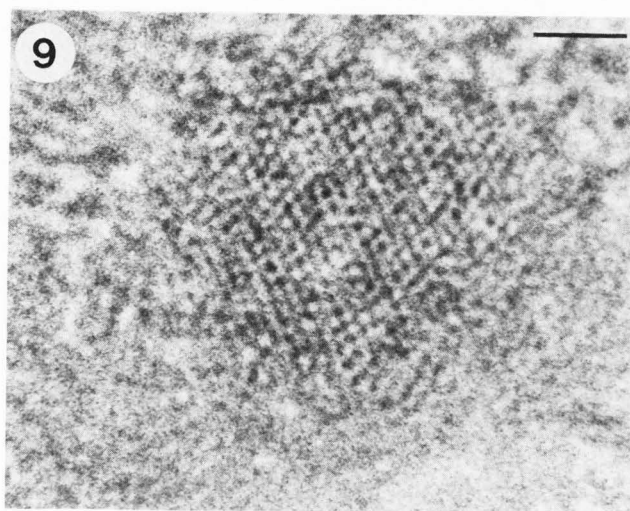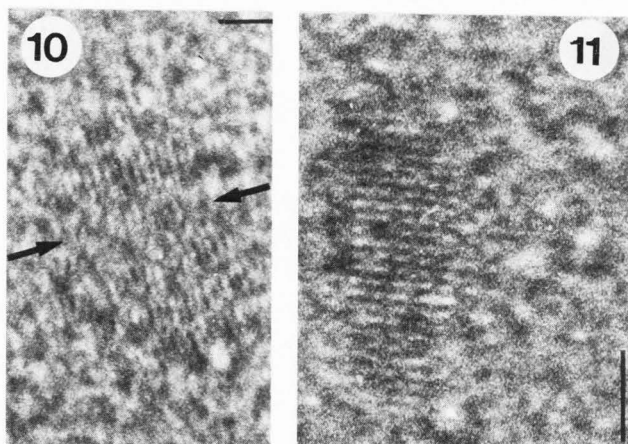unheated human ferritin. Bar = 20A in
each figure.

Figure 10. A 60A core with disordered channel
(arrows) traversing the sets of 2.5A
lattice planes which are discontinuous
within regions of the particle.

Figure 9. Single domain crystal (65A) with
lattice fringes (2.7A) of varying
intensity.

Figure 11. Single crystal core (50A long) showing
growth anisotropy; suggesting growth
along the inner surface of the protein
shell.

The uniqueness of the ferritin structure
arises from the metabolic requirement to organise
and utilise dissolved iron at concentrations and
pH levels which induce precipitation of
potentially toxic solid phases. Not only is iron
solubilised by micelle encapsulation but
homeostatic control is also maintained. The
study of ferritin therefore provides an important
example of biological control of solid state
reactions which involve the formation and
organization of inorganic solids in biological
time and space.

The first high resolution electron microscopy
study of the ultrastructure of horse ferritin
cores utilised dark field imaging techniques
(Massover and Cowley 1973). The results showed
that the iron(III) oxide core was micro-
crystalline, usually single domain but
occasionally multidomain in nature, with a unit
cell based on a four layer repeat of hexagonally
close-packed oxygen atoms with variable
interstitial occupancy of Fe(III) ions, in
agreement with the model by Towe and Bradley
(1967) for the mineral, ferrihydrite ($5Fe_2O_3$
$9H_2O$). Later work using scanning transmission
electron microscopy and microelectron diffraction
confirmed these results (Isaacson and Ohtsuki,
1980). A more detailed investigation using HRTEM
has recently been reported (Mann et al. 1986a).
HRTEM was used to study the ultrastructure of
individual ferritin cores isolated from
vertebrate (human), invertebrate (limpet,
Patella vulgata) and bacterial (Pseudomonas
aeruginosa) sources. Structural similarities and
differences in the cores of these iron storage

proteins are important factors which need to be
examined since they reflect the mechanistic
processes of mineral formation in these
biological systems and may ultimately be related
to functional adaptation. For example, structural
and compositional parameters will have a marked
influence on the rates of storage and
mobilization of iron by the ferritin molecule and
hence on its role in iron homeostasis.

Heat-treated (70°C in a water bath for 5
minutes) and unheated, unstained ferritin cores
from both normal and thalassemic spleens were air
dried onto EM grids and showed lattice fringes
which indicated a predominance of single crystal
domain particles (figure 9). Single crystalline
cores were observed for particles with dimensions
spanning a particle size distribution of 50-70A.
Two dimensional lattice images ('dot-patterns')
were occasionally imaged possibly indicating the
three-dimensional nature of the iron oxide cores.
Fringes were generally low in contrast against
the carbon background of the substrate film but
modulations in the intensity of the lattice
images could be resolved within the individual
crystallites. Discontinuities in fringe patterns
were often observed within the central region of
the cores and occasionally channels of disordered
material could be imaged traversing the particles
between sets of lattice fringes (figure 10). In
some cores, fringes were recorded which indicated
a marked anisotropy in crystal growth resulting
in elongated particles (figure 11). In contrast
to the heat-treated human ferritins, lattice
images of unheated cores showed single domain

crystallites often associated with non-crystalline regions within the same particle (figure 12). It is possible that these apparently non-crystalline regions are in fact crystalline domains misoriented with respect to the electron beam.

Iron(III) oxide-containing human hemosiderin particles were also studied by HRTEM (Mann et al. 1986a). This material is generally thought to be derived from ferritin by lysosomal degradation of the protein shell. The high resolution images indicated that the human hemosiderin particles were structurally related to the human ferritin cores showing similar low contrast lattice fringes within single domain crystallites.

In contrast, limpet and bacterial ferritins showed very few lattice fringes when studied by HRTEM. Limpet cores imaged with resolvable lattice fringes contained crystalline domains with dimensions in the range of 30-50A (figure 13). Bacterial ferritin cores showed only incoherent fringe patterns either with lamella-like structures in which the fringes were convoluted across the particles (figure 14) or structures in which the ordering was extremely short-range (often 10-20A).

Although structural artefacts caused by local electron beam were not totally eliminated the above results show unequivocally the fundamental difference in the crystallographic nature of ferritin mineral cores isolated from human, limpet and bacterial sources. Factors governing this change in crystallochemistry will include the rate of oxidation of Fe(II) on entry into the protein cavity and the subsequent mechanisms of growth of the Fe(III) solid phase. These factors will be dependent on local redox and pH conditions, ionic concentrations (influx and efflux rates) and binding sites at the protein interface. For example, rapid oxidation of Fe(II) will kinetically favour amorphous and poorly-ordered ferrihydrites. Another factor which may be important is the much higher inorganic phosphate level in the bacterial iron-containing core (Mann et al. 1986a), in consequence this protein contains hydrated iron(III) phosphate micelles rather than the hydrated iron(III) oxide phase of vertebrate proteins.

The HRTEM results show that human ferritin cores are essentially single crystals with extensive structural and stoichiometric irregularities (as evidenced by the marked variations in intensity of the images). The growth of a single crystal within the protein cavity requires development of the mineral core at the protein interface. The clustering of glutamate residues at the B-helix interface (Ford et al. 1984) could provide the necessary electrochemical micro-relief to act as a possible nucleation zone. Similar zones will be present at symmetry-related positions within the molecule, but growth from one zone will be favoured over the other regions once a critical nucleus has been established, since the growth process then becomes autocatalytic and spatially localised resulting in single domain crystals.

Lattice images such as those in figure 11

indicate anisotropy in crystal growth that may arise through growth of the iron oxide crystals along the inner surface of the protein shell. Further evidence for growth at the protein interface is provided by images of cores showing centres of low electron density (figure 10, and Issacson and Ohtsuki, 1980).

Limpet teeth. The radula of the common limpet (Patella vulgata) is about 7 cm long and contains over 200 transverse rows of teeth which are extensively mineralized with the iron(III) oxide, goethite (α-FeOOH) (Lowenstam 1962). Transmission electron microscopy, electron diffraction and energy-dispersive X-ray analysis have been used to study the structure, morphology, composition and organization of biominerals within the teeth (Mann et al. 1986b). Both goethite and poorly-ordered iron-containing phases were observed. In addition the goethite crystals were deposited in the form of thin fibrous strands (15-20 nm width) which developed into acicular single crystals often showing marked growth distortions along the [001] direction. HRTEM has been used to study the structural nature of the poorly-ordered material and the local order within immature and mature goethite biocrystals (St Pierre et al. 1986). Fibrous particles isolated from fractured early maturing teeth by grinding in a pestle and mortar followed by ultrasonic dispersion in distilled water showed lattice images corresponding to the goethite crystal structure, with the [001] direction running parallel to the fibre axis. In general the lattice fringes were continuous throughout the crystals indicating the single crystalline nature of these initially deposited biomineral components. Many crystals showed evidence for lattice fringe discontinuities and ill-defined edges (figure 15) and mosaic fringe patterns (figure 16) indicating extensive irregularities in crystal thickness. Some crystals, however, appeared to have well ordered smooth surfaces. Granular material of variable composition (Mann et al. 1986b) was also studied. Lattice images recorded at thin edges of this material clearly revealed the microcrystalline and polycrystalline nature of this phase (figure 17). Lattice fringes were consistent with goethite interplanar d spacings and domain sizes were often of the order of 5 nm.

Mature goethite crystals were also studied. Figure 18 (inset) shows a lattice image of the end of a mature goethite crystal showing marked crystal growth distortions, whereas figure 18 shows the enlarged lattice image obtained from the area delineated in the inset micrograph. Lattice fringes are continuous throughout the particle indicating that the complex and irregular morphology is generated by the growth of an essentially perfect single crystal of goethite.

On the basis of these results a working hypothesis for crystal growth of iron oxides within the limpet tooth matrix has been proposed (St Pierre et al. 1986). The growth of these crystals from solution must be sufficiently slow to prevent domain or intergrowth formation (Cornell et al. 1983) and must be significantly influenced by the local biochemical environment
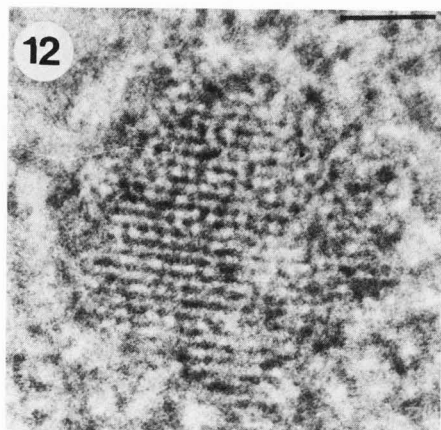
Figure 12. Unheated core (60A) with extensive disordered region contiguous with a single crystal domain (2.7A fringes).
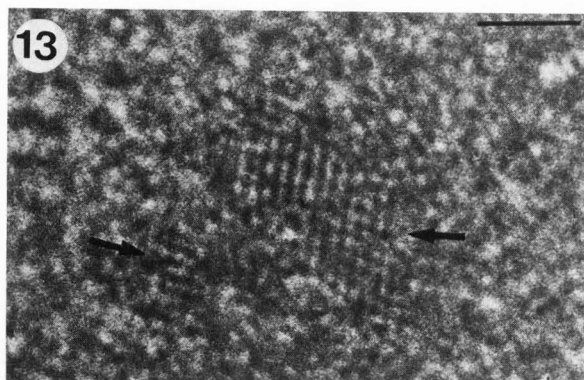

Figure 13. Lattice image of a limpet ferritin core. Growth of a crystalline phase can be seen at two different locations within the core (arrows), possibly at the protein interface. Fringe spacing ca 3 A. Bar = 20 A.
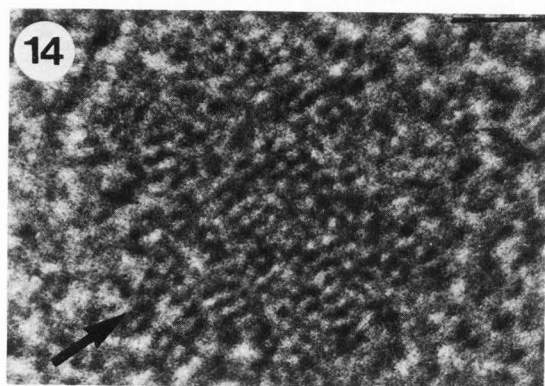

Figure 14. Lattice image of a bacterial ferritin core (ca 65A) showing incoherent lamella-type structures running parallel to the direction marked by the arrow. Bar = 20A.

to account for the marked crystal growth anisotropy. One possibility is that a change in pH or redox across the tooth boundary wall could be responsible for nucleation along the inner wall surface. Growth of the nucleus could then proceed along a concentration profile parallel to the wall surface generated by a continual flux of Fe into the tooth. In this way the initial crystals could be oriented apposed to the wall

Figures 15-17. Lattice images of goethite and granular material from early maturing limpet teeth. Bar in all figures = 5 nm.

Figure 15. Fibrous goethite crystal showing uneven edges and marked discontinuities (arrow) in lattice fringes (2.8A = (011)).

Figure 16. Mosaic fringe pattern (arrows) from a fibrous immature goethite crystal. Fringe spacing is 3.4A (120).

Figure 17. Thin edge of granular material showing local crystalline (goethite) domains. Lattice fringes are 2.6A (021).
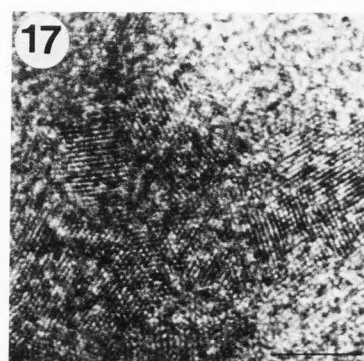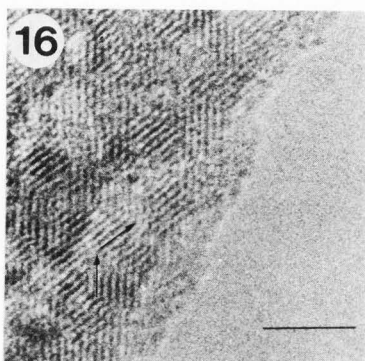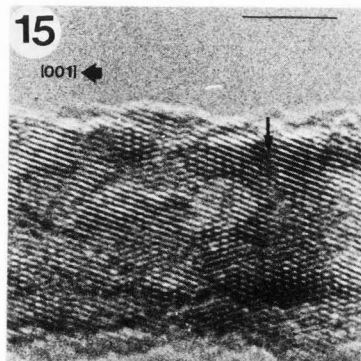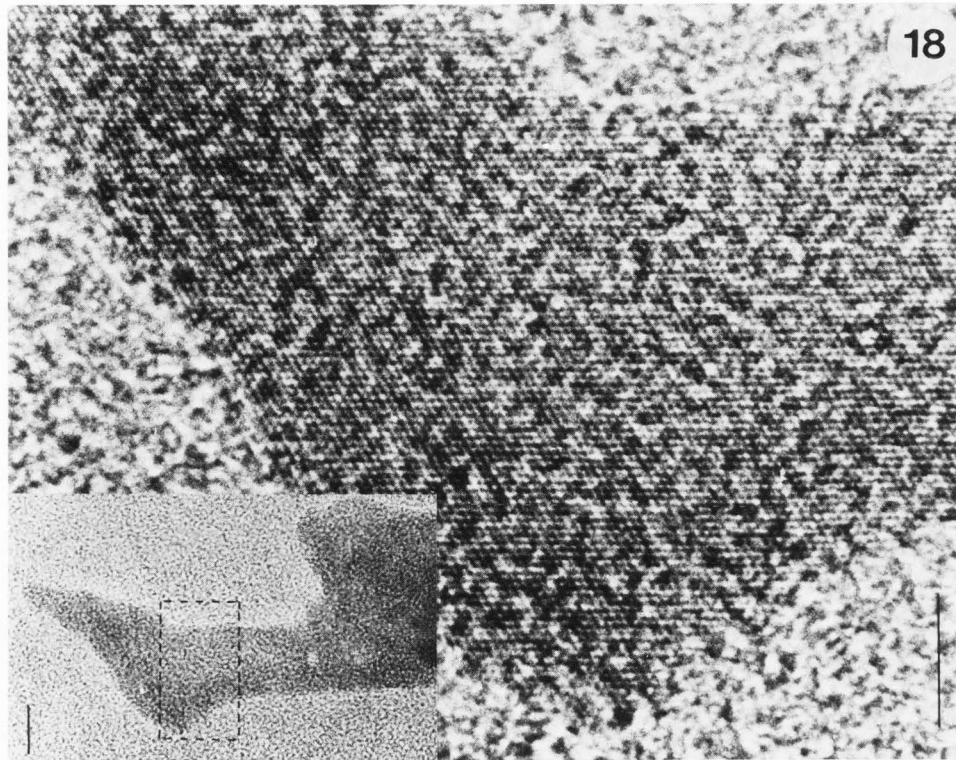
Figure 18. HRTEM image of a mature goethite crystal isolated from limpet teeth showing continuous (040) (2.5A) and (021) (2.6A) fringes throughout the crystal area shown in the inset (box). Bar = 5 nm. Inset; lattice image of the end of a mature goethite crystal exhibiting irregular morphology. Bar = 10 nm.

with the favoured growth direction ([001)] extending parallel to the tooth surface.

Maturation of the goethite crystals occurs primarily by increases in thickness resulting in well formed acicular crystals (Mann et al. 1986 b). However, many crystals show remarkable morphological distortions although as figure 18 shows, such distortions are not associated with structural imperfections in the crystal lattice or domain boundaries. A possible explanation for these crystal forms is that they represent the presence of spatial constraints in the crystallization environment such that the crystals grow to fill the space made available to them within the biological tissue. Since the goethite crystals are closely associated with organic filaments throughout the cusp (Mann et al. 1986b) it is possible that spatial deviations in the organic matrix are ultimately reflected in the morphology of the growing goethite crystals. Thus the organization of matrix components within the teeth may be paramount in the control and organization of inorganic crystallization reactions.

Calcium Phosphate. Calcium phosphate is the major inorganic mineral formed in higher organisms comprising the inorganic component of bone, cartilage, dentine and enamel. The elucidation of the ultrastructure of this material is of great importance in the understanding of control processes in the crystal growth of these biological materials. HRTEM is an excellent technique for such studies, providing information at the nanometre level concerning the relationship of inorganic-organic interactions during crystal formation, crystallographic orientation, ion-exchange properties (through determination of structural inhomogeneities), biomechanical properties and pathological processes such as dental caries and bone resorption.

Human tooth enamel. Human tooth enamel has an inorganic chemical structure and composition approximate to the hexagonal form ($P6_3/m$) of the mineral hydroxyapatite ($Ca_5(PO_4)_3OH$). This phase accounts for 96% by weight of the material, the remainder comprises two major classes of enamel proteins, the amelogenins and the enamelins. The

biological apatites are non-stoichiometric, often with a high carbonate impurity which results in increased structural disorder and changes in the unit cell size (McConnell 1973). Recent investigators (Nelson et al. 1983; Bres et al. 1985) have used HRTEM to study the crystallographic ultrastructure of human tooth enamel at the atomic level. A point-to-point resolution of 2.5A was used with a large objective aperture to allow n-beam lattice imaging of the projected apatite structure. These studies involved the simulation of computer images under a range of defocus and sample thickness conditions allowing a detailed investigation of the projected charge potential to be undertaken.

In the work of Nelson et al. (1983) lattice images from both synthetic and biological carbonated (tooth enamel) apatites, aligned in the [0001] and [$\bar{1}2\bar{1}0$] crystallographic directions, showed good agreement with computer images generated from multislice calculations using the program of Lynch and O'Keefe (1972). The contrast of lattice images recorded on highly substituted carbonated materials was reduced relative to the stoichiometric hydroxyapatite. This may be due to changes in the electron scattering factors on replacement of Ca^{2+} by Na^+ and PO_4^{3-} by CO_3^{2-}. Alternatively the non-stoichiometric materials may contain a significantly large number of point defects providing a diffuse background to the images.

Both beam-induced and nonradiolytic crystallographic disorder have been observed in inorganic and biogenic crystals (Nelson et al. (1983)). Unfortunately there were problems in identifying the numbers of crystal defects in the samples studied due to their critical dependence on crystal thickness and orientation. An unequivocal correlation between crystallographic disorder and increased carbonate content was therefore not possible. However the synthetic carbonated phases and human enamel both showed finely textured surface irregularities which may explain their high rates of dissolution and ion-exchange. No evidence of domain structure was observed in the high resolution lattice images.

Bres et al. (1985) have extended the work of Nelson et al. (1983), matching lattice images of human enamel hydroxyapatite viewed along the [0001], [$\bar{1}2\bar{1}0$], [$1\bar{2}13$], [$1\bar{1}00$] and [$\bar{4}510$] directions with computer-calculated images of the stoichiometric hexagonal form of the mineral hydroxyapatite. Because of the complexity of the hydroxyapatite unit cell the lattice images rarely showed a one-to-one correspondence with the actual atomic structure potential. For example, images recorded along the [0001] zone under conditions of -10 nm defocus and 3 nm crystal thickness showed hexagonal patterns which bear little relationship to the atomic structure projected in this direction. Recording of images under different conditions (-35 nm defocus and 15 nm thickness) gave results in which the tunnel sites could be visualized but no atomic structure details could be clearly resolved (figure 19). However, the clear correspondence of calculated
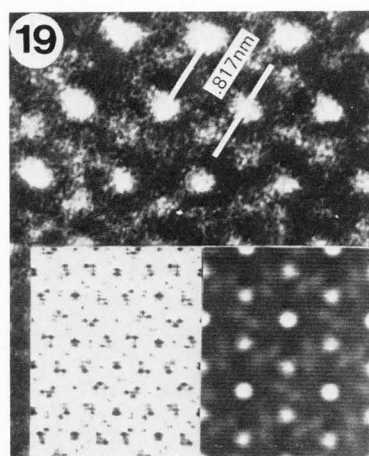

Figure 19. Image of an enamel crystal viewed down [0001] under conditions of -35 nm defocus and 15 nm thickness. Inset (bottom left); projected charge density image for hydroxyapatite. Inset (bottom right); computer image calculated for hydroxyapatite at the above defocus and thickness conditions. Spacing of 8.17 A corresponds to ($10\bar{1}0$). (Bres et al. 1985.)
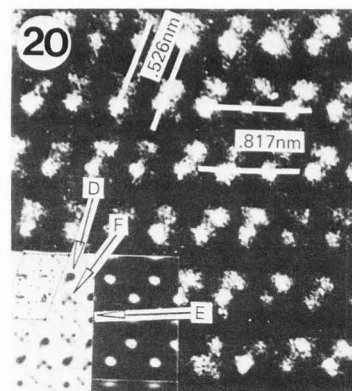

Figure 20. Enamel crystal viewed down the [$1\bar{2}13$] direction. Insets (as above). Values for defocus and thickness are -100 nm and 9 nm respectively. Site D has two Ca, one P and three O atoms; site E has two Ca atoms; site F has three Ca atoms. Spacing of 5.26A corresponds to ($10\bar{1}1$). (Bres et al. (1985)).

and experimental lattice images using the stoichiometric hexagonal hydroxyapatite crystal structure coordinates indicate that the human enamel material is very similar in structure to its inorganic counterpart.

Lattice images recorded in the [$1\bar{2}13$] zone clearly showed the disposition of certain atom clusters in this projection (figure 20). The white dots in the experimental image correspond to a cluster with two phosphorus, one calcium and

three oxygens (site D). In contrast, images recorded in the [$\bar{1}2\bar{1}0$] and [$1\bar{1}00$] zone generally showed only the presence of tunnels in the structure. Several images taken in the [$\bar{1}2\bar{1}0$] zone of projection showed inexact correspondence between experimental and computed images even when tilt considerations were taken into account. In some negatives both good and poor correspondence was observed in different areas of the same crystal. Also, because of the twofold screw axis parallel to [0001] in the stoichiometric hydroxyapatite space group (P6₃/m) diffraction into the 0001 reflection is kinematically forbidden. Even under conditions of double diffraction the (0001) lattice fringes should be weak in intensity. Reference to figure 21 clearly shows a strong (0001) fringe indicating that a two-fold screw axis is not present in this region of the crystal structure. The authors (Bres et al.1985) conclude that whilst many parts of the human enamel crystals can be identified as hexagonal hydroxyapatite, other regions are clearly different. One possibility is that the substitution of tetrahedrally coordinated phosphate by trigonal planar carbonate groups introduces localised structural distortions which change the local crystal symmetry from hexagonal to monoclinic. The existence of this monoclinic phase in enamel from hydroxyapatite may have importance in the bioelectric effects of tooth growth (Basset et al.1964).

Bres et al.(1984) have also used HRTEM to study the process of carious dissolution of human tooth enamel crystals. During the carious process human enamel crystals undergo anisotropic dissolution parallel to the [0001] direction (Jongebloed et al. 1974). The initial site of dissolution is on an axis parallel to the ($1\bar{1}00$) plane (figure 22) (Voegel and Frank 1977).

HRTEM images were taken along the [$11\bar{2}0$] zone of sectioned crystals in order to study the structural properties of the dissolution zone. Deviations from hexagonal symmetry were observed such as a twin boundary terminating at a partial dislocation of edge component b = 1/2 [0001] after which hexagonal symmetry is retained (figure 23). Similarly, buckling of lattice planes in the absence of any specific crystallographic defect were observed (figure 24). In a crystal with a central core lesion (figures 22b and 25) the undissolved lateral sides (LHS and RHS in figure 25) surround the lighter dissolved central area. The angle between the lines on either side of the central region was measured as 1.75° suggesting the presence of a low-angle tilt boundary within the central core lesion. Because of the kinking of the (0002) fringes in certain areas of the grain boundary the angles between the (0002) and ($1\bar{1}00$) fringes was 89° on the LHS and 91° on the RHS. The crystal therefore does not possess true hexagonal symmetry. The symmetry shown is possibly monoclinic or triclinic. Dislocations within the grain boundary (arrow in figure 25) are probably of the 1/3 <$2\bar{1}\bar{1}0$> type, and were not electron beam induced.

These HRTEM results suggest two distinct growth mechanisms for human enamel crystals. Firstly, the low angle grain boundary could be the crystal initiation site, possibly being also the site of an oriented β-pleated sheet protein which acts as an epitaxial surface for controlled nucleation (Traub et al. 1985). After nucleation the crystal grows parallel to the [0001], [$11\bar{2}0$] and [$1\bar{1}00$] directions. Secondly, two crystals could be nucleated nearly adjacent and slightly tilted with respect to each other. Fusion of the crystals during growth forms the low angle grain boundary. Outward growth of the crystal is then the same as above.

The reverse process of enamel growth, viz dissolution, will be influenced by the extent and number of crystallographic defects in the material. HRTEM studies have identified twin boundaries, localised lattice buckling and grain boundaries all of which will play an important role in the processes of dental caries.

Calcium carbonate. Calcium carbonate phases are deposited in bacteria, protozoa, algae, higher plants and invertebrates (Lowenstam 1981). They are also formed, although less widespread, in vertebrates. Three major structural polymorphs have been identified in biological systems; calcite, aragonite and vaterite, although there is also evidence for the monohydrate phase, amorphous phases and an extensive range of Ca/Mg carbonate solid solutions. The calcite structure is related to the NaCl structure by compression along the triad axis giving rise to a rhomobohedral unit cell. In contrast, the aragonite structure is related to the NiAs structure by compressing along the hexad axis resulting in an orthorhombic unit cell. Vaterite is similarly related to the NiAs structure but retains the hexagonal symmetry. Ca^{2+} ions in this structure can be considered to be coordinated to eight oxygens (six at 2.4A, and two at 2.9A) in contrast with the six coordinate Ca of calcite and aragonite.

Two biological systems have been studied in detail by HRTEM; (a) calcite and aragonite crystals in the inner ear receptors of the rat, frog and fish, and (b) calcite formation in a marine unicellular alga Emiliania huxleyi.

Gravity sensors. The inner ears of all vertebrates contain mineral deposits located over sensory areas in the vestibular portion of the membranous labyrinth. These deposits function as detectors of changes in linear acceleration and thus act as gravity sensors. Except for the cyclostomes, which utilize calcium phosphate deposits, the inner ear minerals occur as one or more polymorphs of calcium carbonate. In many organisms the deposits form as a multitude of minute (ca 10µm) crystalline appearing structures called otoconia ('ear-dust'). In bony fishes, however, the deposits occur as large, single mineral masses called otoliths ('ear-stones'). Otoconia of cold blooded vertebrates consist of aragonite whereas warm blooded animals form calcite deposits. Otoliths are nearly always aragonite in structure.

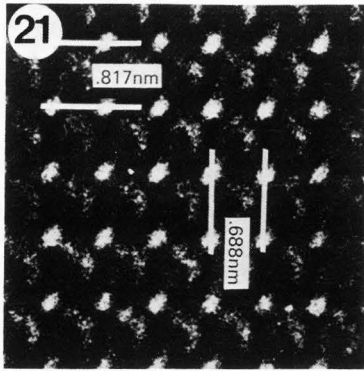There has been much controversy over the

Figure 21. Image of an enamel crystal viewed down [1̄21̄0]. The (0001) spacing (6.88A) is very strong compared with (0002). No computer image could be calculated for hexagonal hydroxyapatite which was comparable with the experimental image. (Bres et al. (1985)).
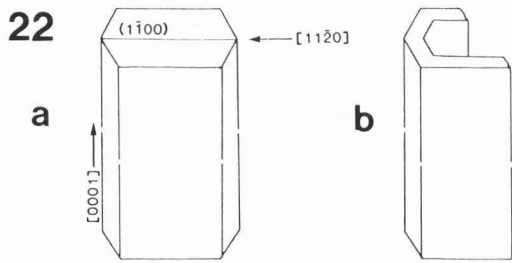

Figure 22

a Diagram showing the morphology of an enamel crystal and corresponding crystallographic directions; b, carious dissolution occurs along the (1100) plane resulting in crystals with a central lesion (see figure 25). (Adapted from Bres et al. 1984).
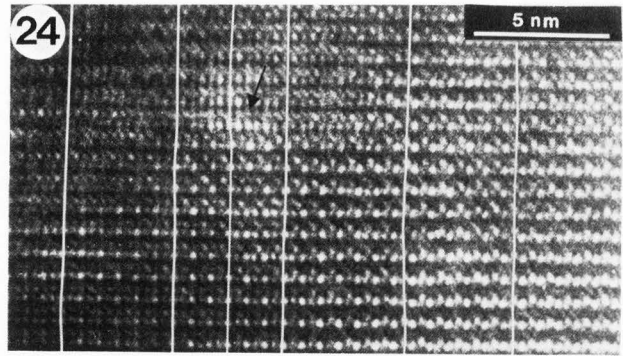
Figure 24. Enamel crystal imaged along [112̄0]. The white lines correspond to buckled lattice planes. The arrow marks a possible dissolution site (region of intense buckling). (Bres et al. (1984)).
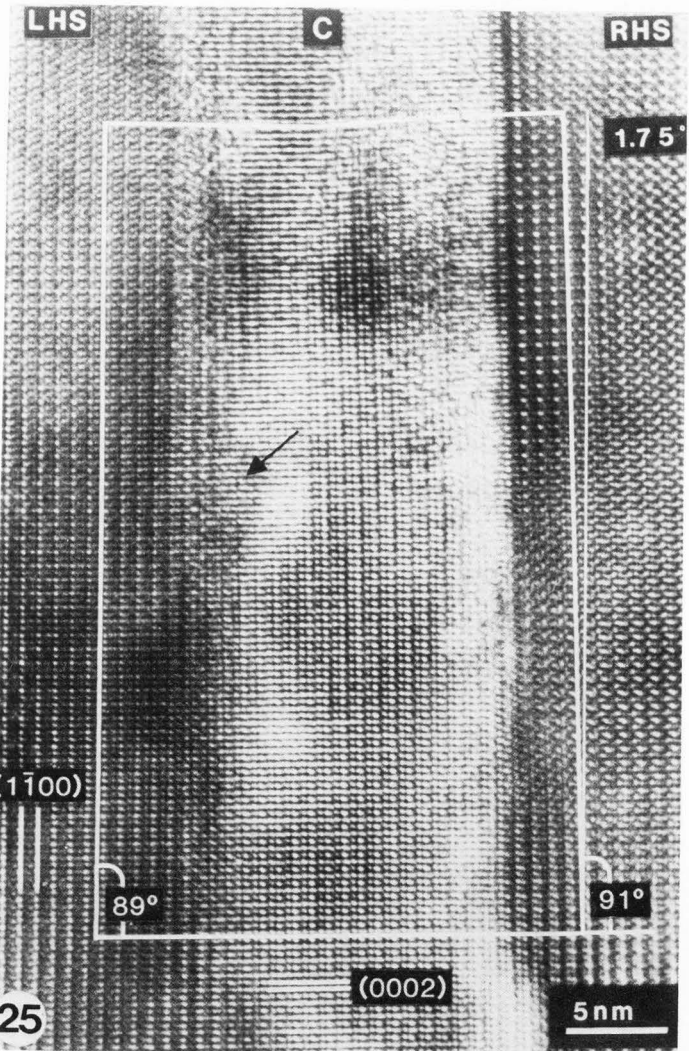

Figure 23. Enamel crystal imaged along [112̄0] showing a twin boundary and edge dislocation (Bres et al. (1984)).

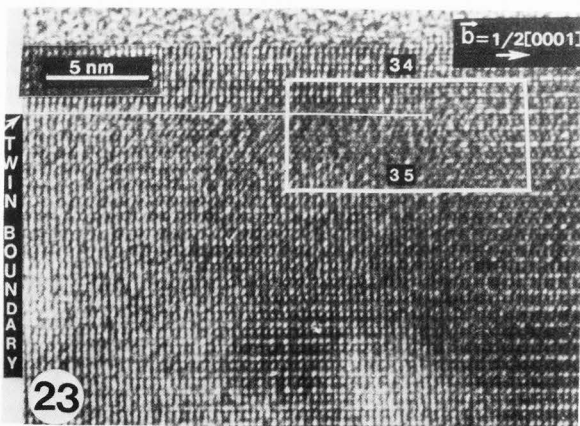Figure 25. Enamel crystal with a central lesion (C) imaged along [112̄0]. For details see text. (Bres et al. (1984)).

precise crystallochemical nature of inner ear deposits. Otoliths appear to be polycrystalline deposits. Although they differ in size and shape among various species of bony fish they all show daily incremental growth and major rings of annular growth (Dunkelberger et al. 1980). Otoconia, in contrast, show an evolutionary trend toward small, discrete, elongated structures with pointed ends that average 10µm in birds and mammals. Each unit has an apparent three-fold symmetry characteristic of single crystals of calcite. The planar end faces are inverted through the centre of the crystal so that the otoconia have the approximate morphology of a rhombohedron.

The extent to which the outer morphology of otoliths and otoconia coincides with their crystallographic properties has been investigated by Carlstrom (1963), who studied 58 different species representative of the vertebrate series using X-ray powder diffraction, optical and polarized light microscopy. He stated that otoliths were polycrystalline as were most otoconia in fishes, but that the otoconia of vertebrates from lung fish through to mammals were single crystals. This is in contrast to an earlier result (Carlstrom and Engstom 1955) which showed that crushed human otoconia yielded hexagonal platelets, suggesting that the overall structure might be a composite of highly ordered subunits. Recently, Ross et al. (1976) showed that the Miller indices of large human otoconia were (100)-type, defining the specific calcite rhombohedron involved. The weight of the crystallographic data, then, supports the conclusion that otoconia largely correspond to single crystals, as also indicated by their morphologies.

This conclusion is, however, in disagreement with embryological data. Salamat et al. (1980) showed that foetal rat otoconia develop in at least two stages and have distinct central and peripheral zones. The growth pattern occurred as a multiple seeding of the inorganic phase along with, or within, an organic substrate. The end faces formed only at a late stage as the microcrystals merged and the adult morphology became apparent. The extent to which the adult otoconium corresponded to a crystallographically defined single crystal was questioned by Nakahara and Bevelander (1979), who suggested on the basis of their ultrastructural study of foetal mouse otoconia that a hexagonal, organic array is initially deposited and then needle-shaped crystals grow within this template, culminating in a unit with many regularly arranged, needle-shaped crystallites, giving rise to a 'multi-iso-oriented' crystal. Later work from Nakahara et al.(1981) showed a cross-like orientation of overall growth, described by the authors as a roughly radial pattern with a crystal-free zone in the centre of the crystal .

HRTEM has been used with an aim to resolve the problem of the degree of three-dimensional periodicity of otoconia and otoliths. Fish (plaice) otoliths (aragonite) frog (aragonite) and rat (calcite) otoconia have been studied in detail by HRTEM (Mann et al. 1983a). The results were compared directly with HRTEM investigations of mineralogical standards of calcite and aragonite.

Each sample, both biogenic and inorganic, was prepared by crushing to a fine powder in a mortar followed by examination in the electron microscope. The inorganic standards yielded a wide range of crystallites with uneven dimensions and distinct crystallographic edges. In contrast, the crushing of the biogenic minerals resulted in rounded crystallites approximately 0.1µm in diameter.

Electron diffraction patterns generated by the fragments from each sample fell into distinct groups (table 1).At least five crystal faces were recognised for each of the five samples and an immediate observation was that the biominerals frequently do not expose the same faces as the geological minerals when crushed. Mineral aragonite was always observed to expose the (010) face, which is the twin plane of the mineral; the aragonitic biominerals, however, also exposed a series of other faces with almost the same incidence; the (001) face in particular becoming exposed. This difference was more marked in the calcitic minerals. Iceland spar shattered to give exclusively high index faces, with (211) and (421) especially common. The rat otoconia, however, showed a high predominance of the (001) face, although some high index faces were also seen. These observations were confirmed by a study of the lattice images of the five samples.

Table 1

Identification of calcium carbonate crystal faces exposed by fracturing

	Index of exposed face	001	010	011	100	111	211	401	421
Mineral									
Calcite	Inorganic	2	–	–	–	–	4	3	5	2
	Rat	10	–	–	–	3	3	–	1	–
Aragonite	Inorganic	–	5	–	–	–	–	–	–
	Fish	3	4	–	–	–	–	–	–
	Frog	4	4	3	1	–	–	–	–

Lattice images were taken of both inorganic and biogenic calcite (rat otoconia) fragments. Electron diffraction patterns were also recorded before and after the recording of lattice image micrographs and showed no changes after exposure indicating the stability of calcite under the experimental conditions used. Fragments from the rat otoconia were often platelets with curved edges and approximately 50-100nm in size. Lattice imaging and electron diffraction patterns revealed that the platelets were single crystals (figures 26 and 27) although some stacking faults were occasionally observed. These units are the
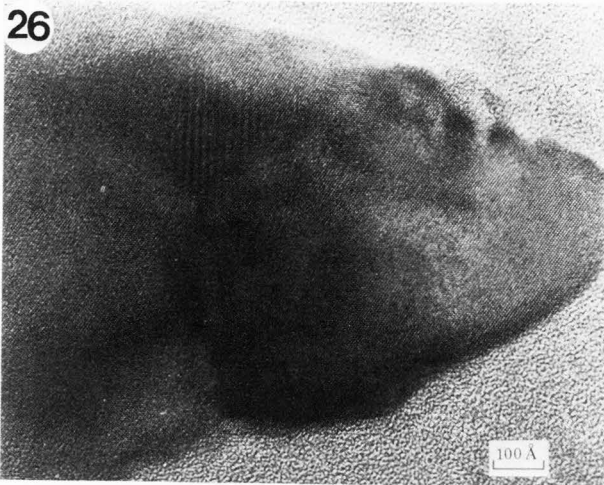
100 Å

Figure 26. HRTEM image of a fragment of calcitic
rat otoconium imaged along [421]. The
fragment is a well-ordered single
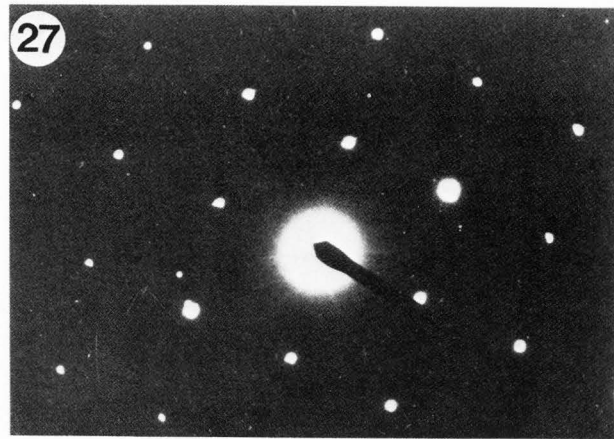crystal. Note the rounded edges.

Figure 27. Selected area electron diffraction
pattern [421] zone) of the fragment
shown in figure 26.

fundamental components from which the bulk
otoconia structure is generated. Each single
crystallite must undergo controlled nucleation
and growth, as shown by the high degree of
perfection in the lattice images. The initial
nucleation centre for each crystallite is
possibly at an organic core formed within a
cellular vesicle (Salamat et al. 1980). The
direction and extent of growth is subsequently
controlled by the organic material in which the
nuclei are embedded. In this way single
crystallites are nucleated in vesicles and
continually exocytosed into an extracellular
matrix. The organization of this matrix then
determines the accretion of the primary
crystallites such that the crystallites become
oriented along radial lines that fan out until
their edges evolve into a continuous bulk crystal
face which is then inhibited from further
development. The combination of HRTEM results
(Mann et al. 1983a) and sectioning studies
(Nakahara et al. 1981) thus gives strong evidence
for the 'multi-iso-oriented' crystalline nature
of otoconia in which the inorganic calcite and
organic phases are in close contact. Although the
final structure has the appearance of a bulk
calcite single crystal this reflects the degree
of spatial ordering of primary crystallites
rather than the intrinsic periodicity of a bulk
crystalline phase.

Fragments (ca 100nm) of biogenic aragonite
from frog otoconia were also shown to be single
crystallites by lattice imaging and electron
diffraction (Mann et al, 1983a). However, unlike
the inorganic aragonite fragments which were also
studied, the biogenic material was unstable under
the electron beam. Small areas of amorphous
material about 50 Å diameter were observed within
the single crystalline domains (figure 28). A
similar phenomenon was also observed for biogenic
aragonite fragments derived from fish otoliths.
Under prolonged exposure biogenic aragonite
electron diffraction patterns showed additional
spots indicating a lowering of crystal symmetry
to a primitive lattice. This modification
suggests a loss of minor components from the
crystal lattice without altering the geometry of
the Ca ions. Chemical analysis revealed the
presence of Na, Sr, Mg and P within the native
otolith structure (Mann et al. 1983a). Thus the
amorphous regions in figure 28 probably
correspond to localised centres of these
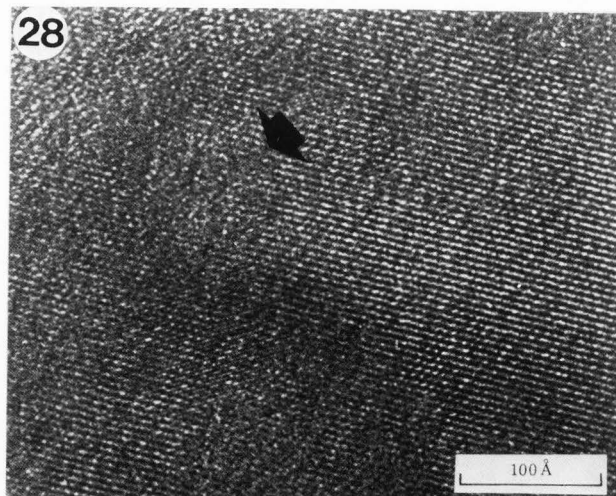interstitial ions.

100 Å

Figure 28. HRTEM image of a fragment of aragonite
from frog otoconia showing localised
amorphous domains (arrow).

Algal Shields. Certain marine unicellular algae, for example Emiliania huxleyi, synthesize an elaborate extracellular shield comprising an intricate network of delicately sculptured oval shaped calcite plates. The morphology of these plates, termed coccoliths, varies in different species. In E.huxleyi the coccoliths are composed of a radially arranged array of crystalline segments each consisting of flattened lower element, a hammer-shaped upper element and a vertical central element. The vertical element connects the other two regions and forms part of the wall of a central cylinder in each coccolith.

Electron microscopical studies on coccolith biosynthesis in E.huxleyi have been carried out by several workers (Wilbur and Watabe (1963), Klaveness (1972). Calcification occurs within specialised intra-cellular vesicles which are closely apposed to the nuclear envelope and which are continuous with a system of anastomising tubes termed the reticular body. The first stage of biosynthesis involves the formation of a polysaccharide-rich organic plate apposed to the nuclear envelope. The nucleation sites for calcification are at the rim of this plate. Rhombohedral crystallites are initially formed which subsequently grow in lateral, medial and distal directions to form the complete segments of each coccolith. Crystal growth along the basal elements follows the line of the organic plate whereas no preformed organic structures have been observed in the upper elements. However, in all stages of calcification the enclosing vesicle membrane roughly parallels that of the forming mineral indicating a process of mutual interaction between the inorganic and organic phases. When mature, the coccoliths are extruded from the cell and organised into an extracellular shield.

HRTEM has been used to study the ultrastructure of coccolith elements separated by ultrasonication. Watabe (1967) proposed, using electron diffraction, that each radial segment in the coccolith was a single calcite crystal of unique and novel morphology. HRTEM studies (Parker et al. 1983), in contrast, have clearly shown that there are different ultrastructural details according to the position within the radial element. Lattice images of the basal plate (lower element) were readily obtained due to the thinness of this structure. When oriented flat on the EM grid both images and electron diffraction patterns clearly showed the structure to be a single crystal oriented in the [421] zone. The projected charge density in this zone under conditions of optimum defocus was calculated and the computer generated image compared closely with the lattice image (figures 29 and 30). The Ca spacing in this zone corresponds to 3.85A (012)/(112). Why this face should be always developed parallel to the organic plate remains to be resolved. It is possible that the 3.85A distance fits a regularly spaced net of Ca binding sites on the polysaccharide plate which thus acts as an epitaxial surface for controlled mineralization.

In contrast, HRTEM images of the irregular-shaped upper elements revealed that these structures were not single crystals but comprised arrays of microcrystals often 300-500A in size (figure 31). The difference between these results and Watabe's electron diffraction work (Watabe 1967) has been suggested by Parker et al. (1983) to be in the fact that Watabe did not consider the arcs in his patterns which arise from the upper elements. However, Parker et al. (1983) were limited in their high resolution study by a restriction of 10° on their tilt stage.

An additional observation in the above HRTEM study was the occasional appearance of triangular patterns of lattice fringes emanating from a single point (figure 32) indicating the presence of multiple nucleation sites. A particularly large number of such centres were observed at the junction of the hammer-like cross pieces in the upper element suggesting that these may be growth sites for these elaborate and complex structures.

In summary, HRTEM has revealed that the upper and lower elements of coccoliths are formed by quite different processes each emanating from the central elements. Unfortunately, the central elements could not be studied as they remained intact within a close ring after sonication, thereby being too thick for lattice imaging. The role of the organic plate may be paramount in controlling the growth of the single crystalline base plate. In contrast, the microcrystalline upper elements lack such a substrate and appear to be formed by the accretion of preformed crystallites.

Amorphous biominerals. Since there can be no sharp boundaries between crystalline and amorphous materials but only a gradual lowering of the degree of structural order from full translational symmetry to order at the nearest neighbour level, many so-called amorphous materials may comprise domains of short range order randomly organised within the bulk structure. The extent of structural definition is thus critically dependent on the experimental techniques available. For example, whereas statistical techniques such as X-ray and electron diffraction when applied to amorphous solids may show only weak diffuse diffraction maxima, HRTEM, on the other hand, can reveal directly local short range order.

Amorphous biominerals are of particular importance since they not only require different biological control processes of formation and organization compared with their crystalline counterparts but are often precursors to more thermodynamically stable crystalline states. For example, the presence and role of amorphous calcium phosphate as a precursor to bone hydroxyapatite has raised much heated discussion. Also, because amorphous biominerals are kinetically stabilised they undergo rapid ion/molecular exchange properties which may play a critical role in homeostatic control, for example, of Ca and Fe levels in vertebrates.

Only two amorphous biominerals have been studied to date using HRTEM, (a) hydrated silica and (b) calcium phosphate.
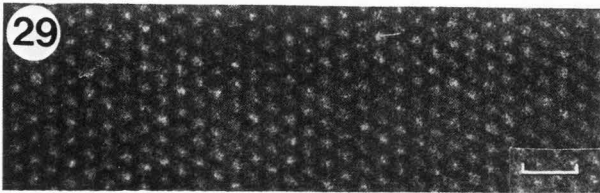
Figure 29. HRTEM image of basal plate enlarged to reveal the hexagonal pattern of the [421] zone of calcite. Bar = 10A (Parker et al. 1983).

Figure 30. Computer generated lattice image of the calcite [421] zone at defocus = -65 nm. (Parker et al. 1983).
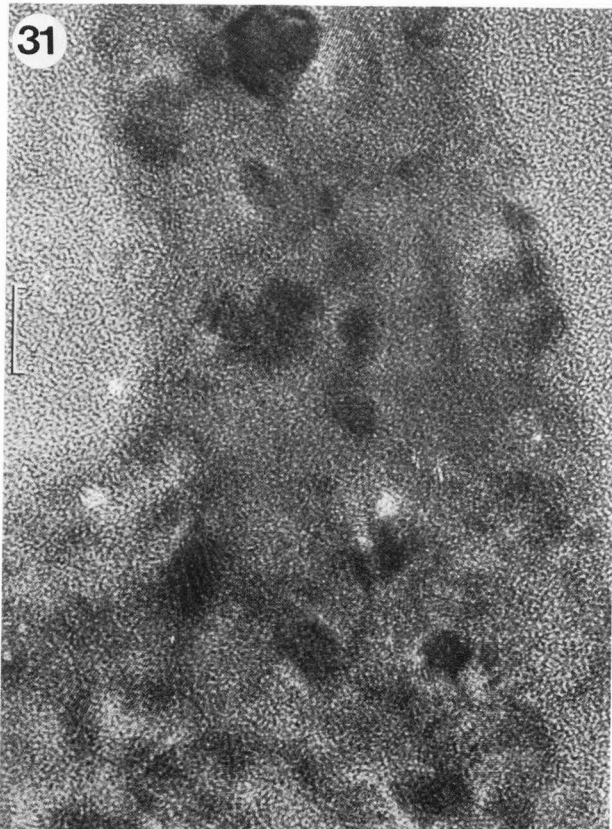

Figure 31. HRTEM image of the 'head' region of an upper element showing the microcrystalline nature of these structures. Bar = 100A (Parker et al. 1983).

Silica rods and spicules. HRTEM has been used to study the structural nature of biogenic silica from Protozoa (Stephanoeca diplocostata Ellis (Mann and Williams 1982) and plants (Phalaris canariensis L. (Mann et al. 1983b).

Stephanoeca diplocostata Ellis is a unicellular marine choanoflagellate which has been successfully established in culture (Leadbeater 1979a). The cells comprise a colourless protoplast which is lodged in a basket-like casing (the lorica) constructed of 150-180 silica costal strips. The rods are approximately 3μm in length, 50 nm in width and have a radius of curvature similar to that of the cell wall. New costal strips are produced in advance of mitosis within long thin vesicles in the peripheral cytoplasm and then released sideways through the plasmalemma into the cavity of the posterior lorica chamber. Bundles of rods are then transferred to the top of the collar until sufficient strips to form a new lorica have been accumulated. Cell division then proceeds, the juvenile taking the accumulation of supernumerary strips as it leaves the parent lorica and assembling its own lorica within 2-3 minutes (Leadbeater 1979b).

Figure 33 shows a HRTEM image recorded from a siliceous costal strip in this marine choanoflagellate (Mann et al, 1983b). The rod is imaged across a hole in the formvar EM grid so there is no background noise from the carbon-coated film contributing to the image detail. Detailed examination of images such as figure 33 revealed only irregular incoherent fringes in all areas of the siliceous biomineral.
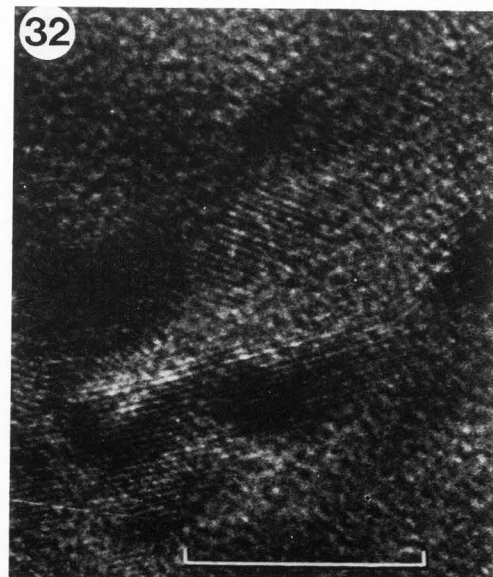

Figure 32. HRTEM image of the upper element close to the interface with the central element. A triangular pattern of lattice fringes can be observed indicating a possible multiple nucleation site. Bar = 100A. (Parker et al.1983).
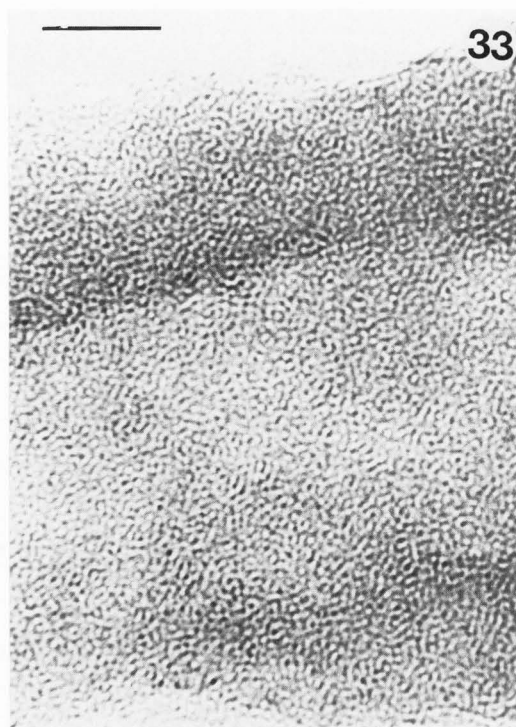
Figure 33. HRTEM image of a costal strip in an intact lorica of Stephanoeca diplocostata. Bar = 10 nm.

Computer simulation studies based on pattern recognition showed no conclusive evidence for regular ordering of local clusters of Si-O bonds. No short range order could be determined extending above 10A (approximately three Si-O-Si units). Interpretation of the fine structure below the limit was difficult due to the thickness and focus effects on image formation.

Similar results were obtained from the silica spicules which surround the lemma of the canary grass Phalaris canariensis (Mann et al, 1983b).

These HRTEM results indicate that the biogenic silica structures are based on a random network of SiO_4 tetrahedral units connected through covalently linked Si-O-Si bonds of variable bond angle rather than the alternative model for an amorphous material, viz a micro-crystalline/cluster structure composed of a random array of microcrystalline polyhedra of various dimensions.

Casein micelles. There has been much controversy over the precise structural nature of the inorganic material of the natural casein micelle of cow's milk. The micelle is a colloidal calcium phosphate-citrate complex in intimate association with several phosphoproteins. The colloidal particles are formed from an aggregation of smaller 25A subunits. EXAFS measurements (Holt et al. 1982) indicated a structure for the calcium phosphate phase closely akin to brushite, $CaHPO_4.2H_2O$, in its short-range order. Alternatively, it has been suggested (McGann et al. 1983) on the basis of infrared spectroscopy and of a determination of
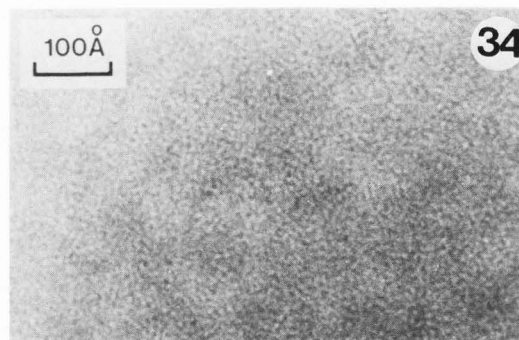

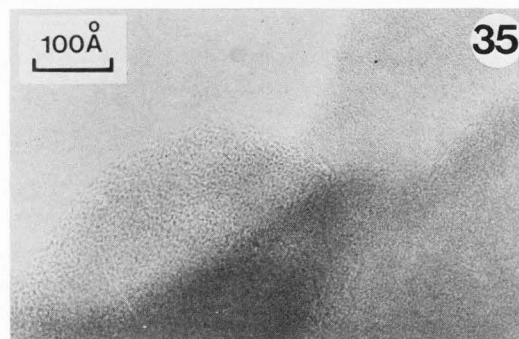Figure 34. HRTEM image of washed casein micelles showing no evidence for structural order.

Figure 35. HRTEM image of digested micellar calcium phosphate showing only amorphous regions.
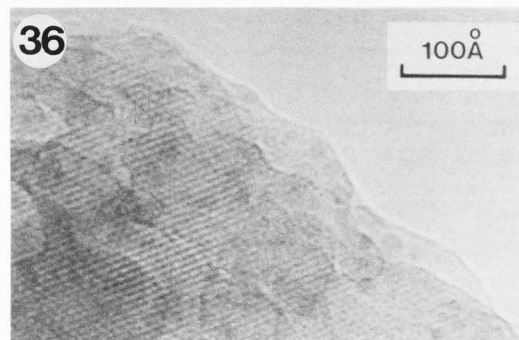
Figure 36. HRTEM image of commercial brushite showing fringes corresponding to (111) and (020) d spacings, of 3A and 7.6A respectively.

radial distribution functions that the material is similar in nature to an amorphous Mg-containing tricalcium phosphate characterised as a precursor of crystalline hydroxyapatite.

HRTEM of the micelles (Lyster et al. 1984) showed only non-periodic images (figure 34) from the thin edges of the micelles. A further sample containing digested, protein-free material was also investigated and gave similar incoherent lattice images (figure 35). In contrast,

commercial brushite showed a wide range of periodic lattice spacings (figure 36) indicating that this material was stable in the electron beam and that the casein micelles images did not arise from beam-damaged brushite material. These results indicate that there are no crystalline phases in the casein micelle and that the material has no long range order beyond 10-15A. The HRTEM and EXAFS results can be accommodated through a model which invokes a calcium phosphate nearest-neighbour configuration close to that in brushite but with no translational order above 15A.

Conclusions

This paper has attempted to place into perspective the role played by HRTEM studies in the investigation of the structure and formation of biogenic inorganic solids. It is clear that this approach has been very successful in probing the ultrastructure of these materials although much further work needs to be done. The combination of HRTEM and high resolution energy – dispersive X-ray analysis in conjunction with a window-less detector configuration will vastly enhance our studies since both structural and compositional parameters of the biomineral phase can be correlated within the same microvolume of sample. Furthermore the use of a window-less detector system will allow mapping of the organic matrices within or enclosing the bioinorganic solids. This will provide information concerning the role of these organic polymers in controlling and determining the number and nature of nucleation sites, crystal growth direction and morphology. Only recently has a combined high resolution analytical electron microscope become commercially available. The above program of exploration is now underway at the University of Bath, UK.

References

Balkwill DL, Maratea D, Blakemore RP. (1980). Ultrastructure of a magnetotactic spirillum. J. Bacteriol. 141, 1399-1408.

Basset CA, Pawluk RJ, Becker RO. (1964). Effects of electric currents on bone in vivo. Nature 204, 652-654.

Blakemore RP, Maratea D, Wolfe RS. (1979). Isolation and pure culture of a freshwater magnetic spirillum in chemically defined medium. J. Bacteriol. 140, 720-729.

Bres EF, Barry JC, Hutchinson JL (1984). A structural basis for the carious dissolution of the apatite crystals of human tooth enamel. Ultramicroscopy 12, 367-372.

Bres EF, Barry JC, Hutchinson JL. (1985). High resolution electron microscope and computed images of human tooth enamel crystals J. Ultrastruct. Res. 90, 261-274.

Carlstrom D. (1963). A crystallographic study of vertebrate otoliths. Biol. Bull. mar. biol. Lab. Woods Mole 125, 441-463.

Carlstrom D, Engstrom A. (1955). The ultrastructure of statoliths. Acta oto-lar 45, 14-18.

Cornell RM, Mann S, Skarnulis AJ. (1983). A high resolution electron microscopy examination of domain boundaries in crystals of synthetic goethite. J. Chem. Soc. Faraday Trans. I. 79, 2679-2684.

Cowley JM, Moodie AF.(1957). The scattering of electrons by atoms and crystals. I. A new theoretical approach. Acta Crystallogr. 10, 609-619.

Dunkelberger DG, Dean JM, Watabe N. (1980). The ultrastructure of the otolithic membrane and otolith in the juvenile mummichog Fundulus heteroclitus. J. Morph. 163, 367-377.

Fischbach FA, Harrison PM, Hoy TG. (1969). The structural relationship between ferritin protein and its mineral core. J. Ultrastruct. Res. 39, 235-238.

Ford GC, Harrison PM, Rice DW, Smith JMA, Treffry A, White JL, Yariv J. (1984). Ferritin : design and formation of an iron-storage molecule. Phil. Trans. R. Soc. Lond. B 304, 551-565.

Frankel RB, Papaefthymiou GC, Blakemore RP, O'Brien W. (1983). Fe_3O_4 precipitation in magnetotactic bacteria. Biophys. Biochim. Acta 763, 147-159.

Holt C, Hasnain SS, Hukins DWL. (1982). Structure of bovine milk calcium phosphate determined by X-ray absorption spectroscopy. Biochim. Biophys. Acta. 719, 299-303.

Hutchison JL, Jefferson DA, Thomas JM. (1977). The ultrastructure of minerals as revealed by high resolution electron microscopy. Chem Soc. Specialist Reports in Surface and Defect Properties of Solids. 6, 320-358.

Isaacson M, Ohtsuki M. (1980). Scanning transmission electron microscopy of small inhomogeneous particles : applications to ferritin. Scanning Electron Microsc. 1980; I: 73-80.

Jongebloed WL, Molenaar I, Arends J. (1974). The dissolution of single crystals of hydroxyapatite in citric and lactic acid. Calcif. Tissue Res. 15, 1-9.

Klaveness D. (1972). Coccolithus huxleyi (Lohmann) Kamptner. I. Morphological investigations on the vegetative cell and the process of coccolith formation. Protistologica 8, 335-346.

Leadbeater BSC. (1979a). Development studies on the loricate choanoflagellate Stephanoeca diplocastata Ellis (I). Protoplasma 98, 241-262.

Leadbeater BSC. (1979b). Development studies on the loricate choanoflagellate Stephanoeca dyplocostata Ellis (II). Protoplasma 98, 311-328.

Lowenstam HA. (1962). Goethite in radular teeth of recent marine gastropods. Science 137, 279-280.

Lowenstam HA. (1981). Minerals formed by organisms. Science 211, 1126-1131.

Lynch DF, O'Keefe MA. (1972). n-beam lattice images. II. Methods of calculation. Acta Crystallogr. A. 28, 536-548.

Lyster RLJ, Mann S, Parker SB, Williams RJP. (1984). Nature of micellar calcium phosphate in cow's milk as studied by high resolution electron microscopy. Biochim. Biophys. Acta 801, 315-317.

Macara IG, Hoy TG, Harrison PM. (1972). The formation of ferritin from apoferritin. Biochem. J. 126, 151-162.

Mann S. (1983). Mineralization in biological systems. Struct. Bond. 54, 125-174.

Mann S. (1985). Structure, morphology and crystal growth of bacterial magnetite. In 'Magnetite biomineralization and magnetoreception in organisms'. (Eds. Kirschrink JL, Jones DS, MacFadden BJ) Plenum, 311-332.

Mann S, Williams RJP. (1982). High resolution electron microscopy studies of the silica lorica in the choanoflagellate Stephanoeca diplocostata Ellis. Proc. R. Soc. Lond. B 216, 137-146.

Mann S, Parker SB, Ross MD, Skarnulis AJ, Williams RJP. (1983a). The ultrastructure of the calcium carbonate balance organs of the inner ear: an ultra-high resolution electron microscopy study. Proc. R. Soc. Lond. B 218, 415-424.

Mann S, Perry CC, Williams RJP, Fyfe CA, Gobbi GC, Kennedy GJ. (1983b). The characterization of the nature of silica in biological systems. J. Chem. Soc. Chem. Comm. 168-170.

Mann S, Frankel RB, Blakemore RP. (1984a). Structure, morphology and crystal growth of bacterial magnetite. Nature 310, 405-407.

Mann S, Moench TT, Williams RJP. (1984b). A high resolution electron microscopic investigation of bacterial magnetite; implications for crystal growth. Proc. Roy. Soc. Lond. B 221, 385-393.

Mann S, Bannister JV, Williams RJP. (1986a). Structure and composition of ferritin cores isolated from human spleen, limpet (Patella vulgata) hemolymph and bacterial (Pseudomonas aeruginosa) cells. J. Mol. Biol. 188, 225-232.

Mann S, Perry CC, Webb J, Luke B, Williams RJP. (1986b). Structure, morphology, composition and organization of biogenic minerals in limpet teeth. Proc. R. Soc. Lond. B. 227, 179-190.

Massover WH, Cowley JM. (1973). The ultrastructure of ferritin macromolecules. The lattice structure of the core crystallites. Proc. Natn. Acad. Sci. USA. 70, 3847-3851.

Matsuda T, Endo J, Osakabe N, Tonomura A. (1983). Morphology and structure of biogenic magnetite particles. Nature 302, 411-412.

McConnell D. (1973). Apatite. Springer Verlag. New York.

McGann TCA, Kearney RD, Buchheim W, Posner AS, Betts F, Blumenthal NC. (1983). Amorphous calcium phosphate in casein micelles of bovine milk. Calcif. Tissue Int. 35, 821-823.

Michaelis L, Coryell CD, Granick S. (1943). The magnetic properties of ferritin and some other colloidal ferric compounds. J. Biol. Chem. 148, 463-480.

Moench TT, Konetzka WA. (1978). A novel method for the isolation and study of a magnetotactic bacterium. Arch. Microbiol. 119, 203-212.

Nakahara H, Bevelander G. (1979). An electron microscope study of the crystal calcium carbonate formation in the mouse otolith. Anat. Rec. 193, 233-241.

Nakahara H, Kakei M, Kunii S. (1981). Fine structure of mouse otolith. Bull. Josai dent. Univ. 10, 333-336.

Nelson DGA, McLean JD, Sanders JV. (1983). A high resolution electron microscope study of synthetic and biological carbonated apatites. J. Ultrastruct. Res. 84, 1-15.

Parker SB, Skarnulis AJ, Westbroek P, Williams RJP. (1983). The ultrastructure of coccoliths from the marine alga Emiliania huxleyi (Lohmann) Hay and Mohler : an ultra-high resolution electron microscope study. Proc. R. Soc. Lond. B 219, 111-117.

Ross MD, Johnson LG, Peacor DR, Allard L. (1976). Observations on normal and degenerating human otoconia. Ann. Otol. Rhinol. Lar. 85, 310-326.

Salamat MS, Ross MD, Peacor DR. (1980). Otoconial formation in the fetal rat. Ann. Otol. Rhinol. Lar. 89, 229-238.

Skarnulis AJ. (1979). A system for interactive image calculation. J. appl. Crystallogr. 1, 636-638.

St Pierre TG, Mann S, Webb J, Dickson DPE, Runham NW, Williams RJP. (1986). Iron oxide mineralization in the radula teeth of the limpet Patella vulgata; Mössbauer spectroscopy and high resolution transmission electron microscopy studies. Proc. R. Soc. Lond. B (in press).

Towe KM, Bradley WF. (1967). Mineralogical constitution of colloidal hydrous ferric oxides. J. Colloid. Interface Sci. 24, 384-392.

Towe KM, Moench TT. (1981). Electron-optical characterization of bacterial magnetite. Earth Planet Sci. Lett. 52, 213-220.

Traub W, Jodaikin A, Weiner S. (1985). Diffraction studies of enamel protein-mineral structural relations. In 'The chemistry and biology of mineralised tissues'. (Ed. Butler WT). Ebsco Media Inc. Birmingham, Alabama, 221-225.

Treffry A, Harrison PM. (1978). Incorporation and release of inorganic phosphate in horse spleen ferritin. Biochem. J. 171, 313-320.

Voegel JC, Frank RW. (1977). Stages in the dissolution of human enamel crystals in dental caries. Calcif. Tissue Res. 24, 19-27.

Watabe N. (1967). Crystallographic analysis of the coccolith of Coccolithus huxleyi. Calcif. Tissue Res. 1, 114-121.

Webb J. (1983). A bioinorganic view of the biological mineralization of iron. In 'Biomineralization and biological metal accumulation' (Ed. Westbroek P and de Jong E W). Reidel, Dordrecht, 413-422.

Wilbur KM, Watabe N. (1963). Experimental studies on calcification in molluscs and the alga coccolithus huxleyi. Ann. N.Y. Acad. Sci. 109, 82-112.

Discussion with Reviewers

N.Rowlands: You state that some biominerals are particularly susceptible to beam damage. Can you give some idea of instrumental conditions necessary for specimen investigation in such cases?

Author: In the case of extremely beam sensitive biominerals we record micrographs essentially "blind",i.e. we establish optimum imaging conditions for the carbon substrate and rapidly move the sample into the viewing area and record the micrograph at as short as possible exposure time. We then repeat the procedure on a new sample area with a small systematic change in the focus conditions.